Gracia, Raquel and Patmore, Nathan J.

Structural, spectroscopic and theoretical studies of diosmium(iii,iii) tetracarboxylates

Structural, spectroscopic and theoretical studies of diosmium(III,III) tetracarboxylates

Raquel Gracia and Nathan J. Patmore

Department of Chemistry, University of Sheffield, Sheffield S3 7HF

Abstract

The preparation of $Os_2(TiPB)_4Cl_2$ (**1**; TiPB = 2,4,6-triisopropylbenzoate) and $Os_2(TiPB)_2(OAc)_2Cl_2$ (**2**) by carboxylate exchange reactions with $Os_2(OAc)_4Cl_2$ is reported. The structure of **1** has been determined by single-crystal X-ray studies, and shows a paddlewheel arrangement of the ligands about the triply bonded diosmium core. Both compounds have magnetic moments at room temperature that are consistent with the presence of two unpaired electrons, and their cyclic voltammograms show a single redox process corresponding to the $Os_2^{5+/6+}$ redox couple. The electronic absorption spectra of **1** and **2** display an absorption at ~395 nm, corresponding to the $\pi(Cl) \rightarrow \pi^*(Os_2)$ LMCT transition, as well as numerous weaker absorptions at lower energy. Density functional theory (DFT) calculations on $Os_2(OAc)_4Cl_2$ at different levels of theory (B3LYP and PBE0) have been used to probe the electronic structure of diosmium tetracarboxylates. The calculations show that these compounds have a $\sigma^2\pi^4\delta^2\delta^{*1}\pi^{*1}$ electronic configuration, and time-dependent DFT was used to help rationalize their optical properties.

TOC Entry

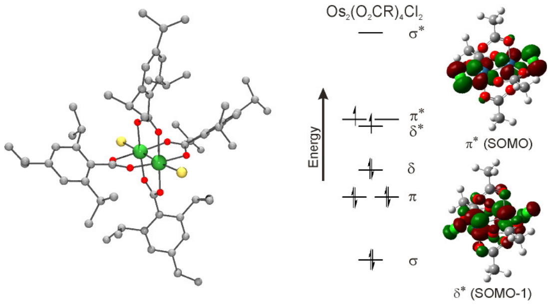

The structural, redox and optoelectronic properties of two disomium tetracarboxylate compounds have been studied, and the results rationalized with the aid of density functional theory calculations.

Introduction

Dimetal paddlewheel complexes contain dimetal cores supported by four bridging ligands such as carboxylates or formamidinates.[1] The unique electronic structure of these species results in complexes with a formal MM bond order of up to 4 and a dimetal core that can exhibit interesting photophysical properties or rich electrochemical behaviour. Diruthenium complexes have been of particular interest in recent years because of their application as catalysts in C-H amination[2] and aerobic oxidation,[3] and as materials with interesting magnetic properties.[4] They have also been shown to be remarkably effective at facilitating electron transfer between redox active centres,[5] making them good candidates for incorporation into molecular wires.[6] By contrast, the chemistry of diosmium paddlewheel complexes, which have a close periodic relationship, has remained somewhat less developed. However the isolation and first structural characterisation of a M_2^{7+} core in $[Os_2(hpp)_4Cl_2]^+$ (hpp = 1,3,4,6,7,8-hexahydro-2*H*-pyrimido[1,2-*a*]pyrimidine),[7] which was characterised by EPR spectroscopy and shown to have a $\sigma^2\pi^4\delta^2\delta^*$ electronic configuration,[8] demonstrates the important contribution that these complexes can make in our understanding of the electronic structure of metal complexes. Diosmium paddlewheel complexes are typically synthesised by ligand metathesis reactions of $Os_2(OAc)_4Cl_2$ and a bidentate ligand such as a carboxylate,[9] amidate,[10] or formamidinate.[11] The axial chloride ligands in $[Os_2(O_2CR)_4Cl_2]$ complexes can be substituted by reaction with HBr.[12] The alkynyl and azido substituted complexes $[Os_2(ap)_4(C_2Y)_2]$ (Hap = 2-anilinopyridine; Y = Ph, Fc, $SiMe_3$) and $[Os_2(DPhF)_4(N_3)_2]$ (HDPhF = *N,N'*-diphenylformamidine) have also been isolated.[13]

Determination of the electronic structure was somewhat more complicated for diosmium tetracarboxylates by comparison to their diruthenium counterparts. Early studies of $[Os_2(O_2C^nPr)_4Cl_2]$ showed a magnetic moment that varied with temperature; decreasing from 1.15 B.M per Os at 300 K to 1.02 B.M. per Os at 188 K.[9,14] This indicated that there were two unpaired electrons in either a $\sigma^2\pi^4\delta^2\pi^{*2}$ or $\sigma^2\pi^4\delta^2\delta^{*1}\pi^{*1}$ electronic configuration. A later magnetic susceptibility study of $[Os_2(O_2CC_6H_4\text{-}2\text{-}C_6H_5)_4Cl_2]$ between 5 - 300 K gave data that could not be modeled based on a $\sigma^2\pi^4\delta^2\pi^{*2}$configuration, ruling this out as a possible ground-state electronic configuration.[15] A model for the temperature dependence of the magnetic susceptibility of diosmium tetracarboxylates was eventually developed by analysis of the magnetic properties of $[Os_2(O_2CCH_3)_4Cl_2]$. The model was based on a $\sigma^2\pi^4\delta^2\delta^{*1}\pi^{*1}$ ground-state configuration incorporating a large zero-field splitting (D = 331 cm^{-1}) that successfully fitted the data between 30 and 350 K.[16] In addition to the complicated magnetic behaviour, the electronic absorption spectra of $[Os_2(O_2CR)_4Cl_2]$ compounds exhibit a number of weak transitions in the visible and NIR region. A detailed solution and solid-state study of the absorption spectra of $[Os_2(O_2CR)_4X_2]$ (R = Me, ^{n}Pr, ^{t}Bu; X = Cl, Br) was used to assign some of these transitions, although a number of visible region transition remain unassigned.

The first aim of this study is to synthesis and characterise diosmium compounds containing the bulky carboxylate ligand 2,4,6-triisopropylbenzoate (TiPB; Scheme 1). We have previously shown that this ligand can significantly distort the diruthenium core in complexes of form $[Ru_2(TiPB)_4]^{0/+}$, resulting in an unusual decrease in Ru-Ru bond length despite increase in bond order.[17] We were intrigued to see if similar effects would be observed in the chemistry of diosmium compounds. The second aim of this study is to probe whether density functional theory calculations can be used to rationalise the structure and ground-state electronic configuration of diosmium tetracarboxylates.

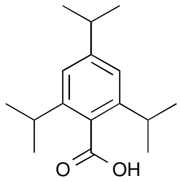

HTiPB

Scheme 1.

Results and Discussion

Synthesis and characterisation

The diosmium tetra-substituted complex $[Os_2(TiPB)_4Cl_2]$, **1**, and the *bis-bis* complex $[Os_2(O_2CCH_3)_2(TiPB)_2Cl_2]$, **2**, were synthesised by carboxylate exchange reactions between $[Os_2(O_2CCH_3)_4Cl_2]$ and HTiPB in refluxing 1,2-Cl_2-C_6H_4 solutions. Both complexes were isolated as brown powders and are soluble in most organic solvents, including hexane. The infrared spectrum for **1** shows two intense bands at 1404 and 1457 cm^{-1} corresponding to the symmetric and asymmetric stretching modes of the bridging carboxylate ligands. More than four stretches are observed in the carboxylate region of the IR spectrum of **2** indicating that ligand stretches are overlapping with the TiPB and OAc ligands. Despite repeated attempts we were unable to grow crystals of **2** in order to determine whether the TiPB ligands are located *trans* or *cis* with respect to one another in the solid state. However, related compounds of form $M_2(TiPB)_2(O_2CR)_2$ (M = Ru,[17b] Mo)[18] exclusively adopt the *trans* arrangement to minimize steric interactions and it is reasonable to assume that same will be the case for **2**. The MALDI-TOF mass spectra show a single peak for both **1** and **2**, with the expected isotope distribution pattern for a diosmium complex. Compounds **1** and **2** are both paramagnetic, with magnetic moments of 2.1 B.M. and 1.9 B.M. at room temperature.

Attempts were also made to isolate the Os(II,III) analogue of **1**, by reaction of **1** with cobaltocene in CH_2Cl_2. This results in the formation of a dark green solution containing [**1**][Co(η^5-C_5H_5)$_2$], but crystals of the compound could not be obtained as it forms an unstable green oil upon removal of solvent. Due to the instablility of [**1**][Co(η^5-C_5H_5)$_2$], we were unable to isolate and fully characterise this complex. The infrared spectrum of freshly prepared sample of shows a shift of the $\nu_{sym}(CO_2)$ and $\nu_{asym}(CO_2)$ stretching frequencies from 1404 cm^{-1} and 1457 cm^{-1} in **1** to 1391 cm^{-1} and 1458 cm^{-1} for [**1**][Co(η^5-C_5H_5)$_2$].

X-ray Crystallography

Crystals of **1** suitable for X-ray diffraction were obtained by slow evaporation of a hexane solution. The structure is displayed in Figure 1, and selected bond lengths and angles are given in Table 1. The structure shows the expected paddlewheel arrangement of the TiPB ligands, and there is a small distortion of the diosmium core from idealised D_{4h} symmetry that presumably minimises steric interactions between the bulky TiPB ligands.

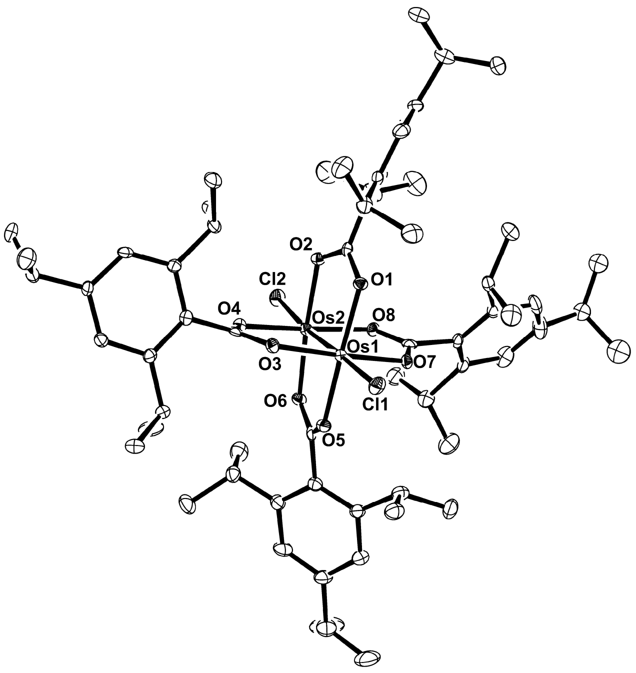

Figure 1. Solid state structure of complex $[Os_2(TiPB)_4Cl_2]$, **1**. Hydrogen and disordered atoms have been omitted for clarity, with thermal ellipsoids drawn at 50% probability level.

Table 1. Selected bond lengths (Å), angles (º) and torsion angles (º) for **1**.

Os1-Os2	2.3276(4)	Os1-Cl2	2.412(2)
Os1-O1	2.030(5)	Os2-Cl1	2.422(2)
Os1-O3	2.013(4)	Os1-Os2-Cl1	174.97(5)
Os1-O5	2.025(5)	Os2-Os1-Cl2	178.64(5)
Os1-O7	2.032(4)	O1-Os1-Os2-O2	5.8(2)
Os2-O2	2.024(5)	O3-Os1-Os2-O4	7.5(2)
Os2-O4	2.038(4)	O5-Os1-Os2-O6	4.6(2)
Os2-O6	2.020(5)	O7-Os1-Os2-O8	7.3(2)
Os2-O8	2.028(5)		

Only four other $[Os_2(O_2CR)_4Cl_2]$ complexes have been structurally characterised, with R = CH_3, C_2H_5, ${}^nC_3H_7$ and 2-PhC_6H_4.[9,15] Pertinent bond lengths and angles for these complexes are included in Table 2 alongside those of **1** for comparison. The average Os-O_{CO2} and Os-Cl bond lengths as well as the Os-Os-Cl angles for **1** are all comparable to those found in other [$Os_2(O_2CR)_4Cl_2$] complexes. The Os-Os bond distance in **1**, 2.3276(4) Å, is the longest found to date, although only by ~0.01 Å. In all of the complexes the Os-Os-Cl bond angle is slightly distorted from linear. Unlike the diruthenium counterparts of **1**, it would appear that the structure of the diosmium core is not significantly perturbed by the bulky TiPB ligand, perhaps because it is slightly larger.

Table 2. Selected bond lengths (Å) and angles (º) obtained for diosmium tetracarboxylates complexes.

Compound	Os-Os (Å)	Os-O_{CO2} (Å)	Os-Cl (Å)	Os-Os-Cl (º)	Ref.
[$Os_2(O_2CCH_3)_4Cl_2$]	2.314(1)	2.01[a]	2.448(2)	177.16(7)	19
[$Os_2(O_2CEt)_4Cl_2$]	2.316(1)	2.01[a]	2.430(5)	176.3(1)	19
[$Os_2(O_2C^nPr)_4Cl_2$]	2.301(1)	2.01[a]	2.417(3)	177.96(10)	9
[$Os_2(2\text{-}PhC_6H_4)_4Cl_2$]	2.3173(6)	2.01[a]	2.386(3)	175.5(4)	15
[$Os_2(TiPB)_4Cl_2$]	2.3276(4)	2.02[a]	2.41[a]	176.8[a]	This work

a) Average value

Cyclic Voltammetry

The cyclic voltammograms of **1** (shown in Figure 2) and **2** were recorded in 0.1 M $Bu_4{}^nPF_6$ CH_2Cl_2 solutions. As expected, they display a single reversible redox process at -0.19 and -0.11 V (vs. Fc/Fc^+) respectively, assigned to the $Os_2{}^{6+/5+}$ reduction. These values are comparable to those recorded for $Os_2(O_2CCH_2CH_3)_4Cl_2$ (-0.03 V) and $Os_2(O_2CCH_2CH_2CH_3)_4Cl_2$ (-0.07 V).[9]

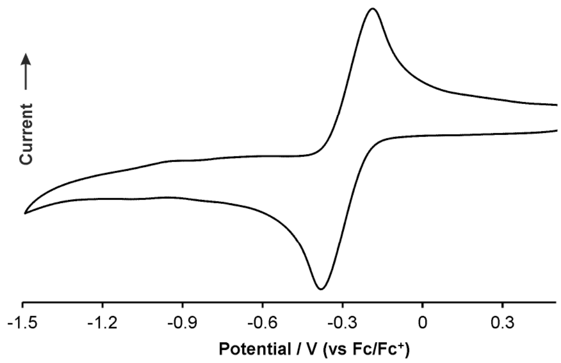

Figure 2. Cyclic voltammogram of **1** in a 0.1 M $N^{n}Bu_4PF_6$ / CH_2Cl_2 solution.

Electronic absorption spectroscopy

The UV/vis spectra of **1** and **2** contain similar features, so we will focus on discussion for **1**. The spectrum of **1** in CH_2Cl_2 is shown in Figure 3 and displays an intense peak at 397 nm. A detailed spectroscopic study on $Os_2(O_2CCMe_3)_4X_2$ (X = Cl, Br) compounds by Miskowski and Gray has assigned this transition to a $\pi(Cl) \rightarrow \pi^*(Os_2)$ LMCT transition. This study also used single crystal polarized absorption spectroscopy to assign weak absorbances at 850 and 1200 nm as the spin-allowed $\delta \rightarrow \delta^*$ and spin-forbidden $\delta^* \rightarrow \pi^*$ transitions respectively. The low-energy region for **1** displays a weak absorbance at 875 nm, which we tentatively assign as the $\delta \rightarrow \delta^*$ transition, where as the expected $\delta^* \rightarrow \pi^*$ transition is too weak and broad to be assigned with any confidence. We also note the appearance of a relatively weak band at 510 nm. This could be due to an impurity in the sample, but it does not disappear after repeated sample recrystallization. We

Whilst the reduced forms of **1** and **2** could not be isolated, we could study the electronic absorption spectrum of $[Os_2(TiPB)_4Cl_2]^-$ (**1**$^-$) spectroelectrochemically at reduced (-20°) temperature (Figure 3). The prominent changes upon reduction is a loss in intensity for the $\pi(Cl) \rightarrow \pi^*(Os_2)$ transition at 397 nm, and a shift in the proposed $\delta \rightarrow \delta^*$ transition to 944 nm. Similar changes were observed in the spectroelectrochemical study of $[Os_2(O_2CC_2H_5)_4Cl_2]^{0/-}$,[20] and the loss of intensity for the LMCT transition is consistent with reduction of Os_2^{6+} to Os_2^{5+}. Switching back to a positive potential at the end of the experiment regenerated **1**, although some bleaching of the $\pi(Cl) \rightarrow \pi^*(Os_2)$ transition indicated a small amount of decomposition (~20%) even at low temperature.

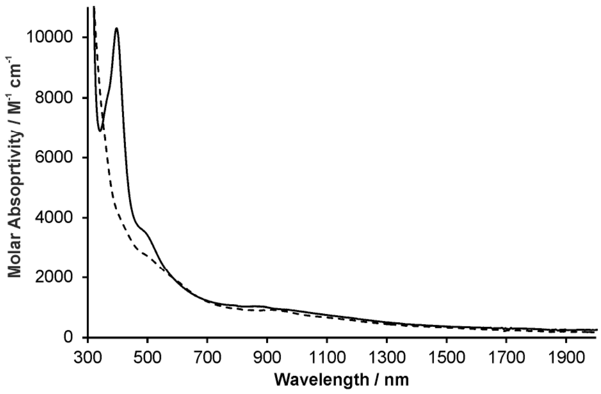

Figure 3. Electronic absorption spectra of **1** (solid) and **1**$^-$ (dashed) in a 0.1 M NBu_4PF_6 / CH_2Cl_2 solution, obtained in a spectroelectrochemical cell at -20ºC.

Computational results

Methodology

Whilst density functional theory (DFT) calculations are now routinely used in the study of dimetal paddlewheel compounds, to the best of our knowledge the only computational studies on diosmium compounds have used SCF-Xα calculations.[15,21] However, there have been a number of DFT studies on closely related diruthenium tetracarboxylates, employing a number of different functional and basis set combinations.[17b,22] A more detailed recent computational study by Roitberg and Cukiernik has used different levels of theory to evaluate electron transfer through coordination polymers containing diruthenium tetracarboxylates.[23]

A recent DFT/TDDFT study on $[Os(N^\wedge N)_2(P^\wedge P)]$ (N^N = 5-(1-isoquinolyl)-1,2,4-triazoles, P^P = bidentate phosphine) compounds using mixed LANL2DZ/6-31G(d) basis sets found that calculations employing the Perdew–Burke–Ernzerhof exchange correlation functional (PBE0) better matched the experimental geometries and absorptions than the B3LYP functional.[24] In order to determine the best functional / basis set combination for diosmium tetracarboxylates we have performed geometry optimisations using BPE0 and B3LYP functionals with the relativistic basis sets SDD or LanL2DZ for osmium, and 6-31G* for the remaining atoms. Calculations on $[Os_2(TiPB)_4Cl_2]^{0/-}$ complexes are too computationally expensive, hence we performed calculations using $[Os_2(O_2CCH_3)_4Cl_2]$ as a model for Os_2(III,III) tetracarboxylates. Full geometry optimization for the triplet state was performed both in vacuum and in dichloromethane solutions using the polarizable continuum model (PCM), with optical transitions calculated using time-dependent DFT. The resulting geometries and calculated energy of the $\pi(Cl) \rightarrow \pi^*(Os_2)$ transition is presented in Table 3, where they are compared with experimental data.

The calculations employing the B3LYP functional model do a reasonable job of modeling the structural parameters, with the calculated Os-Os bond lengths (ranging from 2.356 – 2.378 Å) being only slightly longer than that observed experimentally for $[Os_2(O_2CCH_3)_4Cl_2]$ (2.314(1) Å). Slightly longer calculated MM bond lengths are often seen in DFT studies of dimetal compounds in which basis sets employing an effective core potential are used.[25] However, it is clear that this functional does not do as good a job of modeling the spectroscopic properties; the calculated energy of the $\pi(Cl) \rightarrow \pi^*(Os_2)$ transition is consistently ~0.5 eV too low in energy. By contrast, the PBE0 functional does a much better job of modeling the spectroscopic properties, with the calculated energy of this transition within ~0.2 eV of the experimentally observed values. There is also good agreement between the optimized and experimental structural parameters for this functional. The best correlation between calculated and experimental data is seen for the BPE0 functional with SDD/6-31G* basis sets, and the results from these calculations will be used in the following discussion of electronic structure and spectroscopic assignments.

Table 3. Comparison of calculated and experimental bond lengths (Å), angles (º) and torsion angles (º) for $[Os_2(O_2CCH_3)_4Cl_2]$ in vacuum and solution (CH_2Cl_2).

	B3LYP				PBE0				
	SDD/6-31G*		LANL2DZ/6-31G*		SDD/6-31G*		LANL2DZ/6-31G*		
	Vacuum	Solution	Vacuum	Solution	Vacuum	Solution	Vacuum	Solution	Experimental[a]
Os-Os	2.375	2.356	2.378	2.361	2.350	2.332	2.355	2.332	2.314(1)
Os-O$_{CO2}$[b]	2.07	2.06	2.06	2.05	2.05	2.04	2.01	2.04	2.01
Os-Cl	2.401	2.445	2.418	2.464	2.368	2.408	2.386	2.406	2.448(2)
Os-Os-Cl	162.6	164.8	163.4	165.7	162.0	164.1	162.8	163.4	177.16(7)
O$_{CO2}$-Os-Os-O$_{CO2}$[b]	1.7	1.0	1.5	0.8	1.9	1.1	1.6	1.2	1.5
λ_{max} LMCT (nm)	462 (2.69)	463 (2.68)	470 (2.64)	470 (2.64)	428 (2.90)	425 (2.92)	434 (2.86)	431 (2.88)	392 (3.17)[c]

a) Values obtained from reference [19]. b) Average values. c) Value for $[Os_2(O_2CCH_2CH_3)_4Cl_2]$ in CH_2Cl_2.[9]

Calculated Electronic Structure

There are three possible electronic configurations for $[Os_2(O_2CCH_3)_4Cl_2]$; a singlet ($\sigma^2\pi^4\delta^2\delta^{*2}$) and two triplets ($\sigma^2\pi^4\delta^2\delta^{*1}\pi^{*1}$ or $\sigma^2\pi^4\delta^2\pi^{*2}$). The triplet state for $[Os_2(O_2CCH_3)_4Cl_2]$ was calculated to be 13.4 (vacuum) and 23.7 (solution) kJ mol^{-1} more stable than the singlet state. Whilst these values need to be treated with caution as hybrid functionals such as PBE0 tend to stabilise higher spin states,[26] the results are in agreement with magnetic studies on related Os_2^{6+} species which can be successfully modeled based upon a $\sigma^2\pi^4\delta^2\delta^{*1}\pi^{*1}$ configuration.[16,20,27]

Calculated open-shell frontier MO energy level diagrams for $[Os_2(O_2CCH_3)_4Cl_2]$ are displayed in Figure 4. In both instances the LUMO is the Os_2 π^*, whilst the SOMOs are the Os_2 δ^* and π^* orbitals, giving a $\sigma^2\pi^4\delta^2\delta^{*1}\pi^{*1}$ electronic configuration.[16] Diagrams of these orbitals shown in Figure 5 show strong mixing with π(Cl) and σ(Cl) combinations. Figure 4 shows that the ordering of the MOs is broadly similar in both vacuum and solution, but orbitals are shifted to lower energy in solution. A number of doubly occupied axial chloride π and σ orbitals are found close in energy to the Os_2 δ^* and π^* orbitals. In vacuum, the Os_2 δ orbital is lower in energy than some of the π(Cl) and σ(Cl) combinations, however in solution the Os_2 δ orbital appears at a slightly higher energy than the axial ligand orbitals in the *β* manifold.

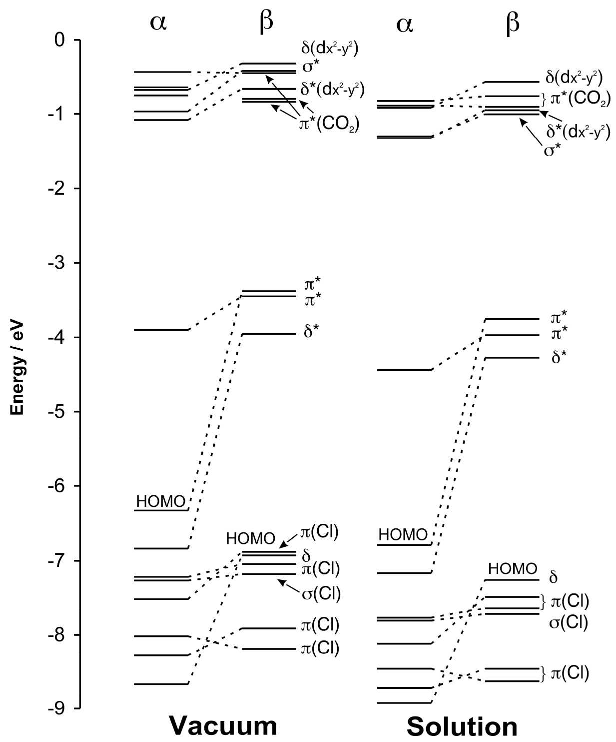

Figure 4. Calculated open-shell frontier MO diagrams for $[Os_2(O_2CCH_3)_4Cl_2]$ in vacuum (left) and CH_2Cl_2 solution (right).

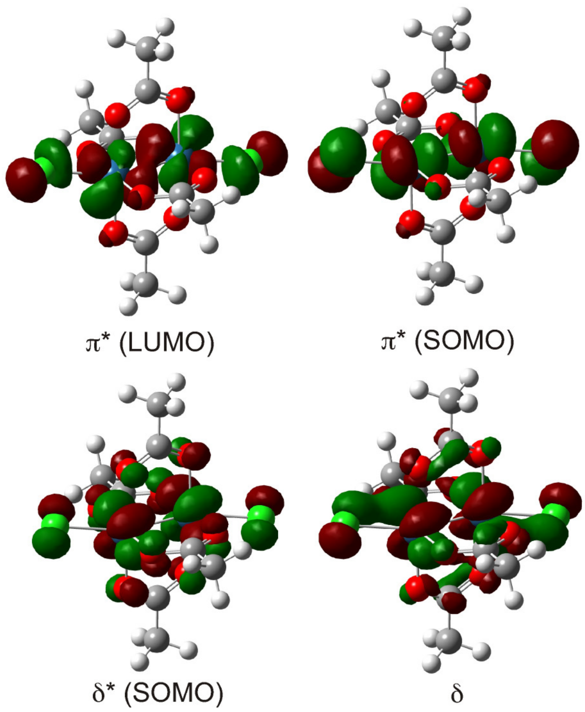

Figure 5. Plots of selected α-MOs for calculated for $[Os_2(O_2CCH_3)_4Cl_2]$ in vacuum (0.04 isosurface value).

TDDFT calculations

The optical transitions for [$Os_2(O_2CCH_3)_4Cl_2$] were calculated in vacuum and solution, and the results are summarized in Table 4. The calculated features of the electronic absorption spectrum [$Os_2(O_2CCH_3)_4Cl_2$] in both vacuum and solution are similar, although they do differ slightly in the calculated transition energies. Given that most experimental data for this type of species is reported in solution we will discuss the solution calculations.

The two lowest energy transitions calculated for [$Os_2(O_2CCH_3)_4Cl_2$] occur at 1572 nm (0.789 eV) and 1350 nm (0.919 eV) , and can be assigned as $\delta^* \rightarrow \pi^*$ and $\delta \rightarrow \delta^*$ transitions respectively. These assignments are consistent with those from the previous experimental study on [$Os_2(O_2CCH_3)_4Cl_2$], in which the two lowest transitions were observed at 1100 nm (1.13 eV) and 850 nm (1.46 eV).[16] The intense transition calculated at 425 nm (2.915 eV; f = 0.1439) is a π(Cl) $\rightarrow \pi^*$ LMCT transition, which corresponds well to the intense transition observed at ~395 nm for [$Os_2(O_2CR)_4Cl_2$] species. The calculations indicate that the weak transitions observed experimentally in the 400 to 700 nm region, but previously unassigned, are likely to correspond to a mixture of π(Cl) $\rightarrow \pi^*$ and σ(Cl) $\rightarrow \delta^*$ LMCT transitions.

Table 4. Calculated transitions (with *f* > 0) for [$Os_2(O_2CCH_3)_4Cl_2$] in vacuum and in solution. Transitions are assigned based on their most significant character.

Vacuum				Solution			
λ, nm	λ, eV	*f*	assign.	λ, nm	λ, eV	*f*	assignment
1326	0.935	0.0011	$\delta^* \rightarrow \pi^*$	1572	0.789	0.0007	$\delta^* \rightarrow \pi^*$
1171	1.059	0.0001	$\delta \rightarrow \delta^*$	1350	0.919	0.0005	$\delta \rightarrow \delta^*$
1049	1.182	0.0004	π(Cl) $\rightarrow \pi^*$	1084	1.144	0.0005	π(Cl) $\rightarrow \pi^*$
779	1.591	0.0002	π(Cl) $\rightarrow \pi^*$	766	1.619	0.0005	π(Cl) $\rightarrow \pi^*$
778	1.594	0.0004	σ(Cl) $\rightarrow \delta^*$	699	1.773	0.0003	σ(Cl) $\rightarrow \delta^*$
670	1.850	0.0005	π(Cl) $\rightarrow \pi^*$	528	2.350	0.0002	π(Cl) $\rightarrow \pi^*$
549	2.256	0.0002	π(Cl) $\rightarrow \pi^*$	425	2.915	0.1439	π(Cl) $\rightarrow \pi^*$
445	2.786	0.0004	π(Cl) $\rightarrow \delta^*$	407	3.047	0.0007	π(Cl) $\rightarrow \delta^*$
428	2.900	0.0860	π(Cl) $\rightarrow \pi^*$	395	3.142	0.0109	π(Cl) $\rightarrow \delta^*$
419	2.959	0.0205	π(Cl) $\rightarrow \delta^*$	373	3.323	0.0208	π(Cl) $\rightarrow \pi^*$

Conclusions

Diosmium compounds containing the bulky carboxylate ligand 2,4,6-triisopropylbenzoic acid have been synthesized, and the solid-state structure of **1** was has been determined by single-crystal X-ray diffraction. The UV/vis spectroscopy and electrochemical studies show that the use of a sterically hindered ligand does not significantly perturb the geometry or electronic structure of the Os_2^{6+} core, although compound **1** does show improved solubility in most organic solvents.

The electronic structure of these diosmium paddlewheel compounds has been rationalized for the first time with the aid of DFT calculations that employ basis sets with a relativistic effective core potential for Osmium. The PBE0 / SDD / 6-31G* combination of functional and basis sets was found to most closely match the structural and optoelectronic properties of diosmium tetracarboxylates. These calculations also support a $\sigma^2\pi^4\delta^2\delta^{*1}\pi^{*1}$ electron configuration for the diosmium core, proposed by Miskowski and Gray on the basis of magnetic studies in 1997.[16]

Experimental

General considerations

Matrix assisted laser desorption/ionization time-of-flight (MALDI-TOF) mass spectrometry was performed using [1,8-dihydroxy-9,10-dihydroanthracen-9-one] (dithranol) as the matrix, prepared as a saturated solution in toluene. Allotments of matrix and sample were thoroughly mixed together; 0.5 mL of this was spotted on the target plate and allowed to dry. IR spectra were recorded as solid samples with a Perkin Elmer Spectrum RX I FT-IR spectrometer equipped with a DuraSamplIR II diamond ATR probe and universal press. Magnetic moments were determined at room temperature using a Sherwood Scientific Magway MSB Mk1 magnetic susceptibility balance. Molar diamagnetic corrections were applied to the magnetic susceptibility data on the basis of Pascal's constants.[28] Electronic absorption spectra were recorded using a Varian Cary 5000 UV-Vis-NIR spectrophotometer. Elemental analyses were carried out by the Microanalytical Service of the Department of Chemistry at Sheffield with a Perkin-Elmer 2400 analyzer. Electrochemical studies were carried out in N_2-purged methanol solutions with 0.1 M [^{n}Bu$_4$N][PF$_6$] as supporting electrolyte. A standard three-electrode system was used with a Pt microdisc and a large surface area Pt wire as the working and counter electrodes, respectively. Potentials were measured in reference to a Ag/AgCl reference, with all potentials quoted for a scan rate of 100 mV s^{-1}. At the end of every experiment, ferrocene was added as an internal standard, with the Fc/Fc^+ couple consistently observed at +0.43 V vs. Ag/AgCl. The UV/vis spectroelectrochemical studies were performed in an optically transparent thin layer electrode cell, in 0.1 M [^{n}Bu$_4$N][PF$_6$] CH_2Cl_2 solutions. Ward and coworkers have previously described the cell setup and temperature control procedures.[29]

All experimental manipulations were performed under an inert atmosphere using standard Schlenk line techniques. Solvents were distilled over an appropriate drying agent prior to use. [$Os_2(O_2CCH_3)_4Cl_2$] was prepared according to literature procedures,[9] and all other chemicals were acquired from commercial sources.

Synthesis of [Os_2(TiPB)$_4Cl_2$], ***1***

A solution of [$Os_2(O_2CCH_3)_4Cl_2$] (0.100 g, 0.14 mmol) and HTiPB (0.360 g, 1.45 mmol) in 1,2-Cl_2-C_6H_4 (50 mL) was refluxed under an argon atmosphere for 16 h. The brown solution was cooled to room temperature, and filtered to remove a dark precipitate. The filtrate was dried *in vacuo*, and the product further purified by redissolving in hexane and filtering again before removing the solvent *in vacuo*. Excess HTiPB was recovered by sublimation at 130 ºC, 10^{-3} Torr, to afford [Os_2(TiPB)$_4Cl_2$] as a brown-yellow powder. Yield = 0.180 g (87%).

Crystals suitable for X-ray diffraction were grown by slow evaporation of a hexane solution. MALDI-TOF-MS: calcd. monoisotopic MW for $Os_2C_{64}O_8H_{92}Cl_2$ 1441.54, found *m/z* 1441.81 (M^+ 100%). IR (cm^{-1}): 2961s, 2929w, 2869w, 1755w, 1695s, 1605s, 1575w, 1457m, 1404s, 1363m, 1260s, 1110m, 1021s, 876m, 791s, 750m. Magnetic moment (solid); μ_{eff} = 2.1 B.M.. $\lambda_{max}(CH_2Cl_2)$ / nm (ε / M^{-1} cm^{-1}): 397 (10,300), 505sh (3340) 875 (1030). Found: C, 52.81; H, 6.24. $Os_2C_{64}O_8H_{92}Cl_2$ requires C, 53.37; H, 6.44%.

Synthesis of [$Os_2(OAc)_2(TiPB)_2Cl_2$], ***2***

A solution of [$Os_2(O_2CCH_3)_4Cl_2$] (0.100 g, 0.14 mmol) and HTiPB (0.072 g, 0.28 mmol) in 1,2-Cl_2-C_6H_4 was refluxed for 14 h. The solvent was removed *in vacuo*, and the product purified by redissolving in dichloromethane and filtering the solution before removing the solvent *in vacuo* to afford [$Os_2(O_2CCH_3)_2(TiPB)_2Cl_2$] as a brown powder. Yield = 0.110 g (74%). MALDI-TOF-MS: calcd. monoisotopic MW for $Os_2C_{36}O_8H_{52}Cl_2$ 1064.16, found *m/z* 993.29 (M-$2Cl^+$ 100%). IR (cm^{-1}): 2963s, 2922m, 2866w, 1712s, 1688s, 1620w, 1604m, 1534m, 1460s, 1440s, 1428w, 1412s, 1396s, 1372w, 1334w, 1197w, 1173m, 1156m, 1111s, 1063s, 1021w, 949w, 902w, 877w, 852w, 831s, 800s. λ_{max}(THF) / nm (ε / M^{-1} cm^{-1}): 380 (3900), 407 (3500), 875 (576). Magnetic moment (solid); μ_{eff} = 1.9 B.M.. Found: C, 41.02; H, 4.97. $Os_2C_{36}O_8H_{52}Cl_2$ requires C, 40.63; H, 4.93%.

Synthesis of [(η^5-$C_5H_5)_2Co$][$Os_2(TiPB)_4Cl_2$], ***3***

A solution of [$Os_2(TiPB)_4Cl_2$] (50 mg, 0.035 mmol) in CH_2Cl_2 was treated with cobaltocene (6.5 mg, 0.035 mmol). The reaction mixture was then stirred at room temperature for 30 minutes, during this time the clear brown solution becomes dark green. The solution was then dried *in vacuo* to obtain an unstable dark green oil that decomposes quickly in the presence of air. IR (cm^{-1}): 2952s, 2916w, 2863w, 1604s, 1569w, 1504w, 1458m, 1391s, 1361m, 1349w, 1319w, 1295w, 1255s, 1156m, 1087s, 1012s, 940m, 875m, 861m, 794s.

X-ray crystallography

Data were measured on a Bruker Smart CCD area detector with Oxford Cryosystems low temperature system. After integration of the raw data and merging of equivalent reflections, an empirical absorption correction was applied (SADABS) based on comparison of multiple symmetry-equivalent measurements.[30] The structures were solved by direct methods (SHELXS-97) and refined by full-matrix least squares on weighted F^2 values for all reflections using the SHELX suite programs.[31] All hydrogens were included in the models at calculated positions using a riding model with U(H) = 1.5 x U_{eq} (bonded carbon atom) for methyl hydrogens and U(H) = 1.2 x U_{eq} (bonded carbon atom) for methine and aromatic hydrogens.

One of the TiPB groups in **1** was disordered over two positions (0.49/0.51 site occupancy), and the atoms associated with the disordered components were refined isotropically. The supplementary crystallographic data for this compound is contained in CCDC 941063.

Table 5. Crystal data for **1**.

Empirical formula	$C_{64}\ H_{92}\ Cl_2\ O_8\ Os_2$
Formula weight	1440.68
Temperature (K)	150(2)
Wavelength (Å)	0.71073
Crystal system, space group	Monoclinic, $P2_1/c$
a (Å)	21.6846(7)
b (Å)	15.5809(5)
c (Å)	19.2799(7)
α (°)	90
β (°)	96.865(2)
γ (°)	90
Volume (Å^3)	96.865(2)
Z, Calculated density (g cm^{-3})	4, 1.480
F(000)	1.480
θ range for data collection (°)	1.61 - 27.46
Limiting indices	-27<=h<=28, -20<=k<=20, -21<=l<=24
Reflections collected / unique	59767 / 14650 [R(int) = 0.0752]
Completeness	to θ = 27.46; 99.0%
Data / restraints / parameters	14650 / 0 / 683
Goodness-of-fit on F^2	1.018
Final R indices [$I > 2\sigma(I)$]	R_1 = 0.0451, wR_2 = 0.0881
R indices (all data)	R_1 = 0.0947, wR_2 = 0.1021
Largest diff. peak and hole (e Å^{-3})	2.144 and -2.191

DFT calculations

Molecular structure calculations on $Os_2(O_2CCH_3)_2Cl_2$ were performed using density functional theory as implemented in the Gaussian03 suite programs.[32] Calculations were performed using either the B3LYP functional[33] or Perdew–Burke–Ernzerhof exchange correlation functional (PBE0),[34] in combination with the effective core potential basis sets LANL2DZ[35] or SDD[36] for Os, and 6-31G* basis set[37] for all other atoms. Unrestricted open-shell calculations were performed in every case. Electrons of alpha and beta spins are independently described which results in a set of orbital energies and molecular orbitals for electrons of alpha spin and another one for electrons of beta spin. Full geometry optimization was performed with C_i symmetry constraints for each functional / basis set combination in both vacuum and in a CH_2Cl_2 solvent cavity using the polarizable continuum model, as implemented in *Gaussian 09*. The results from the PBE0 / SDD / 6-31G* combination most closely matched the experimental data, and the structures in vacuum and solution were confirmed to be the minimum on the potential energy surface by frequency analysis. Electronic absorption spectra were calculated using the time-dependent DFT (TD-DFT) method.

Supporting Information

Calculated atomic coordinates for $Os_2(O_2CCH_3)_2Cl_2$ (both vacuum and PCM solvent model) at the PBE0 / SDD / 6-31G* level of theory.

Acknowledgements

The Royal Society is thanked for the award of a University Research Fellowship (NJP). Dr Anthony Meijer is thanked for computational assistance and Mr Harry Adams is thanked for crystallographic help.

References

1. F. A. Cotton, C. A. Murillo and R. A. Walton, *For a detailed review of this field see.*
2. A. K. M. Long, R. P. Yu, G. H. Timmer and J. F. Berry, *J. Am. Chem. Soc.*, 2010, **132**, 12228.
3. a) N. Komiya, T. Nakae, H. Sato and T. Naota, *Chem. Commun.*, 2006, 4829; b) H. B. Lee and T. Ren, *Inorg. Chim. Acta*, 2009, **362**, 1467; c) C. N. Kato, M. Ono, T. Hino, T. Ohmura and W. Mori, *Cat. Commun.*, 2006, **7**, 673.
4. a) M. Mikuriya, D. Yoshioka and M. Handa, *Coord. Chem. Rev.*, 2006, **250**, 2194; b) T. E. Vos, Y. Liao, W. W. Shum, J.-H. Her, P. W. Stephens, W. M. Reiff and J. S. Miller, *J. Am. Chem. Soc.*, 2004, **126**, 11630; c) B. S. Kennon, J.-H. Her, P. W. Stephens and J. S. Miller, *Inorg. Chem.*, 2009, **48**, 6117; d) M. C. Barral, T. Gallo, S. Herrero, R. Jiménez-Aparicio, M. R. Torres and F. A. Urbanos, *Inorg. Chem.*, 2006, **45**, 3639; e) M. C. Barral, D. Casanova, S. Herrero, R. Jiménez-Aparicio, M. R. Torres and F. A. Urbanos, *Chem. Eur. J.*, 2010, **16**, 6203.
5. a) J.-W. Ying, I. P.-C. Liu, B. Xi, Y. Song, C. Campana, J.-L. Zuo and T. Ren, *Angew. Chem. Int. Ed.*, 2010, **49**, 954; b) G.-L. Xu, R. J. Crutchley, M. C. DeRosa, Q.-J. Pan, H.-X. Zhang, X. Wang and T. Ren, *J. Am. Chem. Soc.*, 2005, **127**, 13354.

6. a) D. Olea, R. González-Prieto, J. L. Priego, M. C. Barral, P. J. de Pablo, M. R. Torres, J. Gómez-Herrero, R. Jiménez-Aparicio and F. Zamora, *Chem. Commun.*, 2007, 1591; b) A. S. Blum, T. Ren, D. A. Parish, S. A. Trammell, M. H. Moore, J. G. Kushmerick, G.-L. Xu, J. R. Deschamps, S. K. Pollack and R. Shashidhar, *J. Am. Chem. Soc.*, 2005, **127**, 10010; c) S. P. Cummings, J. Savchenko, P. E. Fanwick, A. Kharlamova and T. Ren, *Organometallics*, 2013, **32**, 1129; d) J.-L. Zuo, E. Herdtweck and F. E. Kühn, *J. Chem. Soc., Dalton Trans.*, 2002, 1244.
7. F. A. Cotton, N. S. Dalal, P. Huang, C. A. Murillo, A. C. Stowe and X. Wang, *Inorg. Chem.*, 2003, **42**, 670.
8. F. A. Cotton, G. M. Chiarella, N. S. Dalal, C. A. Murillo, Z. Wang and M. D. Young, *Inorg. Chem.*, 2010, **49**, 319.
9. T. Behling, G. Wilkinson, T. A. Stephenson, D. A. Tocher and M. D. Walkinshaw, *J. Chem. Soc., Dalton Trans.*, 1983, 2109.
10. A. R. Chakravarty, F. A. Cotton and D. A. Tocher, *Inorg. Chim. Acta*, 1984, **89**, L15.
11. F. A. Cotton, T. Ren and J. L. Eglin, *Inorg. Chem.*, 1991, **30**, 2559.
12. T. W. Johnson, S. M. Tetrick and R. A. Walton, *Inorg. Chim. Acta*, 1990, **167**, 133.
13. a) Y.-H. Shi, W.-Z. Chen, K. D. John, R. E. Da Re, J. L. Cohn, G.-L. Xu, J. L. Eglin, A. P. Sattelberger, C. R. Hare and T. Ren, *Inorg. Chem.*, 2005, **44**, 5719; b) P. M. B. Piccoli and J. F. Berry, *J. Clust. Sci.*, 2010, **21**, 351.
14. T. A. Stephenson, D. A. Tocher and M. D. Walkinshaw, *J. Organomet. Chem.*, 1982, **232**, C51.
15. F. A. Cotton, T. Ren and M. J. Wangner, *Inorg. Chem.*, 1993, **32**, 965.
16. V. M. Miskowski and H. B. Gray, *Top. Curr. Chem.*, 1997, **191**, 41.
17. a) R. Gracia, H. Adams and N. J. Patmore, *Dalton Trans.*, 2009, 259; b) R. Gracia, H. Adams and N. J. Patmore, *Inorg. Chim. Acta*, 2010, **363**, 3856.
18. M. V. Barybin, M. H. Chisholm, N. J. Patmore, R. E. Robinson and N. Singh, *Chem. Commun.*, 2007, 3652.
19. F. A. Cotton, A. R. Chakravarty, D. A. Tocher and T. A. Stephenson, *Inorg. Chim. Acta*, 1984, **87**, 115.
20. S. M. Tetrick, V. T. Coombe, G. A. Heath, T. A. Stephenson and R. A. Walton, *Inorg. Chem.*, 1984, **23**, 4567.
21. P. A. Agaskar, F. A. Cotton, K. R. Dunbar, L. R. Falvello, S. M. Tetrick and R. A. Walton, *J. Am. Chem. Soc.*, 1986, **108**, 4850.
22. a) B. E. Bursten, M. H. Chisholm and J. S. D'Acchioli, *Inorg. Chem.*, 2005, **44**, 5571; b) M. A. Castro, A. E. Roitberg and F. D. Cukiernik, *Inorg. Chem.*, 2008, **47**, 4682; c) O. V. Sizova, L. V. Skripnikov, A. Y. Sokolov and O. O. Lyubimova, *J. Struct. Chem.*, 2007, **48**, 28.
23. M. A. Castro, A. E. Roitberg and F. D. Cukiernik, *J. Chem. Theory Comput.*, DOI: 10.1021 / ct400179t.
24. J. Su, L. Shi, X. Sun, W. Guan and Z. Wu, *Dalton Trans.*, 2011, **40**, 11131.
25. F. A. Cotton and X. Feng, *J. Am. Chem. Soc.*, 1997, **119**, 7514.
26. M. Reiher, O. Salomon and B. A. Hess, *Theor. Chem. Acc.*, 2001, **107**, 48.
27. F. A. Cotton, K. R. Dunbar and M. Matusz, *Inorg. Chem.*, 1986, **25**, 1585.
28. G. A. Bain and J. F. Berry, *J. Chem. Educ.*, 2008, **85**, 532.
29. S.-M. Lee, R. Kowallick, M. Marcaccio, J. A. McLeverty and M. D. Ward, *J. Chem. Soc., Dalton Trans.*, 1998, 3443.
30. G. M. Sheldrick, University of Gottingen, Germany, 1996.
31. , Bruker Analytical X-ray Instruments Inc., Madison, WI, 1998.
32. M. J. Frisch, G. W. Trucks, H. B. Schlegel, G. E. Scuseria, M. A. Robb, J. R. Cheeseman, J. A. Montgomery Jr., T. Vreven, K. N. Kudin, J. C. Burant, J. M.

Millam, S. S. Iyengar, J. Tomasi, V. Barone, B. Mennucci, M. Cossi, G. Scalmani, N. Rega, G. A. Petersson, H. Nakatsuji, M. Hada, M. Ehara, K. Toyota, R. Fukuda, J. Hasegawa, M. Ishida, T. Nakajima, Y. Honda, O. Kitao, H. Nakai, M. Klene, X. Li, J. E. Knox, H. P. Hratchian, J. B. Cross, C. Adamo, J. Jaramillo, R. Gomperts, R. E. Stratmann, O. Yazyev, A. J. Austin, R. Cammi, C. Pomelli, J. W. Ochterski, P. Y. Ayala, K. Morokuma, G. A. Voth, P. Salvador, J. J. Dannenberg, V. G. Zakrzewski, S. Dapprich, A. D. Daniels, M. C. Strain, O. Farkas, D. K. Malick, A. D. Rabuck, K. Raghavachari, J. B. Foresman, J. V. Ortiz, Q. Cui, A. G. Baboul, S. Clifford, J. Cioslowski, B. B. Stefanov, G. Liu, A. Liashenko, P. Piskorz, I. Komaromi, R. L. Martin, D. J. Fox, T. Keith, M. A. Al-Laham, C. Y. Peng, A. Nanayakkara, M. Challacombe, P. M. W. Gill, B. Johnson, W. Chen, M. W. Wong, C. Gonzalez and J. A. Pople, Gaussian, Inc.
, Wallingford CT, 2004.

33. a) A. D. Becke, *Phys. Rev. A*, 1988, **38**, 3098; b) A. D. Becke, *J. Chem. Phys.*, 1993, **98**, 5648.
34. a) J. P. Perdew, K. Burke and M. Ernzerhof, *Phys. Rev. Lett.*, 1996, **77**, 3865; b) J. P. Perdew, K. Burke and M. Ernzerhof, *Phys. Rev. Lett.*, 1997, **78**, 1396.
35. P. J. Hay and W. R. Wadt, *J. Chem. Phys.*, 1985, **82**, 299.
36. D. Andrae, U. Haeussermann, M. Dolg and H. Preuss, *Theor. Chim. Acta*, 1990, **77**, 123.
37. W. J. Hehre, L. Radom, P. v. R. Schleyer and J. A. Pople, *Molecular Orbital Theory*, John Wiley and Sons, New York, 1986.